JNS

LABORATORY INVESTIGATION

In vitro evaluation of flow diverter performance using a human fibrinogen–based flow model

Cem Bilgin, MD,[1] Esref Alperen Bayraktar, MD,[1] Alexander A. Oliver, BS,[1] Jiahui Li, PhD,[1] Juan R. Cebral, PhD,[2] David F. Kallmes, MD,[1] and Ramanathan Kadirvel, PhD[1,3]

Departments of [1]Radiology and [3]Neurologic Surgery, Mayo Clinic, Rochester, Minnesota; and [2]Center for Computational Fluid Dynamics, George Mason University, Fairfax, Virginia

OBJECTIVE Fibrin deposition represents a key step in aneurysm occlusion, promoting endothelization of implants and connective tissue organization as part of the aneurysm-healing mechanism. In this study, the authors introduce a novel in vitro testing platform for flow diverters based on human fibrinogen.

METHODS A flow diverter was deployed in 4 different glass models. The glass models had the same internal parent artery (4 mm) and aneurysm (8 mm) diameters with varying parent artery angulations (paraophthalmic, sidewall, bifurcation, and slightly curved models). The neck size and area were 4 mm and 25 mm^2, respectively. Human fibrinogen (330 mg/dl) was circulated within the glass models at varying flow rates (0, 3, 4, and 5 ml/sec) with or without heparin, calcium chloride, and thrombin for as long as 6 hours or until complete fibrin coverage of the flow diverter's neck was achieved. Aneurysm neck coverage was defined as macroscopic fibrin deposition occluding the flow diverters' pores. Flow characteristics after flow diverter deployment were assessed with computational fluid dynamics analysis. The effects of flow rates, heparin, calcium chloride, and thrombin on fibrin deposition rates were tested using 1-way ANOVA and the Tukey test.

RESULTS A total of 84 replicates were performed. Human fibrin did not accumulate on the flow diverter stents under static conditions. The fibrin deposition rate on the aneurysm neck was significantly greater with the 5 ml/sec flow rate as compared to 3 ml/sec for all models. The paraophthalmic model had the highest inflow velocity of 48.7 cm/sec. The bifurcation model had the highest maximum shear stress (SS) and maximum normalized shear stress values at the device cells at 843.3 dyne/cm^2 and 35.1 SS/SS_{inflow}, respectively. The fibrin deposition rates of the paraophthalmic and bifurcation models were significantly higher than those of sidewall and slightly curved models for all additive or flow rate comparisons ($p = 0.001$ for all comparisons). The incorporation of thrombin significantly increased the fibrin deposition rates across all models ($p = 0.001$ for all models).

CONCLUSIONS Rates of fibrin deposition varied widely across different configurations and additive conditions in this novel in vitro model system. Fibrin accumulation started at the aneurysm inflow zone where flow velocity and shear stress were the highest. The primary factors influencing fibrin deposition included flow velocities, shear stress, and the addition of thrombin at a physiological concentration. Further research is needed to test the clinical utility of fibrinogen-based models for patient-specific aneurysms.

https://thejns.org/doi/abs/10.3171/2024.4.JNS232567

KEYWORDS flow diverter; aneurysm; fibrin; hemorrhagic stroke; subarachnoid bleeding; vascular disorders

Fibrin is the end product of coagulation cascades and plays a critical role in thrombus formation[1,2] and aneurysm healing after endovascular aneurysm treatment.[2–4] The initial step in the interaction between blood and a flow diverter involves the adsorption of fibrin and proteins onto the surface of the device.[3,4] Subsequently, this adsorbed fibrin can serve as a scaffold for both thrombus formation and the migration of endothelial cells from the adjacent parent vessel. This pivotal event plays a crucial role in determining the durability of aneurysm occlusion.[3,4] While the importance of fibrin in aneurysm healing is well established, predictors of optimal fibrin accumulation on the aneurysm neck and the rationale for differences in patient outcomes after flow diversion remain largely unexplored.

The long-term complete aneurysm occlusion rates consistently stayed under 80% in pivotal flow diversion trials,[5–7] and to date, predicting patients who will benefit from flow diversion remains a challenging task even for

ABBREVIATIONS CFD = computational fluid dynamics; SS = shear stress.

SUBMITTED November 9, 2023. **ACCEPTED** April 10, 2024.
INCLUDE WHEN CITING Published online July 12, 2024; DOI: 10.3171/2024.4.JNS232567.

©AANS 2024, except where prohibited by US copyright law

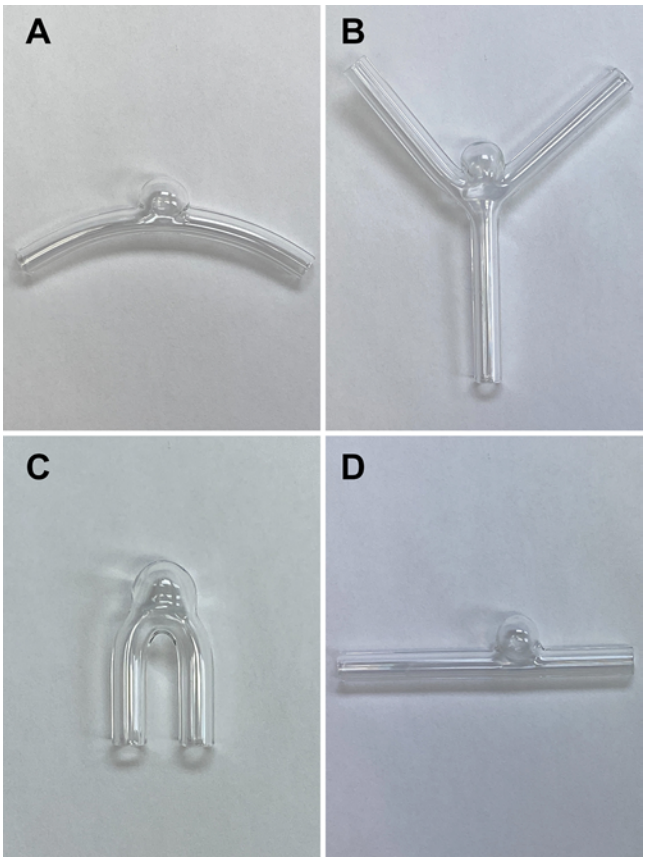

FIG. 1. Glass models. Slightly curved (**A**), bifurcation (**B**), paraophthalmic (**C**), and sidewall (**D**) models are shown. Figure is available in color online only.

experienced neurointerventionalists. Failed flow diversion attempts burden the healthcare system and put patients at risk due to long-term antiplatelet treatment and potential periprocedural complications. Considering the vital role of fibrin in aneurysm occlusion after endovascular treatment, in vitro models focusing on the amount of fibrin accumulation and patterns may be of value for predicting patient-specific outcomes. In this study, we sought to elucidate the primary factors influencing fibrin accumulation on flow diverter stents. Additionally, we aimed to develop a preclinical testing platform utilizing human fibrinogen for flow diverter stents.

Methods

Glass Models

Four different glass models with varying parent artery–aneurysm angulations were used for the experiments (Fig. 1). In all models, the lumen diameter of the parent vessel was 4 mm, and the aneurysm sac was a sphere with a diameter of 8 mm. The center of the aneurysm sac was positioned 1 radius above the center of the apex of the parent vessel in all models. All aneurysm models featured an oval-shaped neck, measuring 4 mm in the short axis and 8 mm in the long axis, with the neck area being 25 mm^2. The paraophthalmic aneurysm model had the curvature of parent artery wrapping 160° around a circle with a radius of 5 mm. The sidewall aneurysm model had a straight parent vessel. The slightly curved aneurysm model had a curvature of parent artery wrapping 80° around a circle with a radius of 50 mm. The bifurcation model had 45° angles between the distal small branches. In the bifurcation model, the distal minor branches measured 2 mm in diameter. Except for the sidewall aneurysm model, aneurysms were positioned at the curvature points in all models.

Benchtop Model and Human Fibrinogen Solution

A cobalt-chromium flow diverter (Fort Wayne Metals) was deployed in the different glass models. The flow diverters were 4.75 mm in diameter and 20 mm in length, and the porosity was 41 pores/mm^2. Next, human fibrinogen concentrate (Fibryga, Octapharma) was circulated within the glass models by using a peristaltic pump in triplicate. Fibryga was specifically chosen over alternative fibrinogen sources such as fresh frozen plasma for two main reasons. First, the Fibryga solution is transparent, enabling real-time visualization of the aneurysm neck. In contrast, fresh frozen plasma's turbid yellow color hinders assessment of gradual aneurysm neck coverage. Second, fresh frozen plasma includes other coagulation factors and a potent anticoagulant, citrate, that can introduce bias and make it impossible to obtain specific results for fibrinogen.

The temperature of the test fluid was consistently maintained at 37°C using a heating bath. To obtain realistic and consistent results, the fibrinogen concentrate was diluted to a physiological concentration of 330 mg/dl in a 100-ml reservoir across all replicates. First, we conducted control experiments under no-flow conditions for all glass models. Next, to examine the impact of the flow rate on fibrin accumulation, we recorded fibrin accumulation times and the characteristics for varying flow rates (0, 3, 4, and 5 ml/sec). Then, using a standardized flow rate of 4 ml/sec, we examined the impact of calcium, thrombin, and heparin on fibrin accumulation characteristics. Calcium (8 mg/dl) and thrombin (0.1 U/ml) were used in physiological concentrations. Furthermore, the concentration of heparin was set at 1 U/ml, which is equivalent to a 5000 IU bolus of intravenous heparin. Aneurysm neck coverage was defined as complete macroscopic closure of the flow diverter's pores.

No-flow control experiments were observed for at least 48 hours. Other experiments were monitored either until there was complete aneurysm neck coverage or for a duration of 6 hours, whichever was shorter. If the aneurysm neck was not completely covered after 6 hours, two independent authors blindly assessed the extent of the coverage. First, two scales were placed perpendicularly along the long and short axes of the aneurysm neck. Then, two authors measured the area covered by fibrin and proportioned it to the area of the aneurysm neck (25 mm^2). In instances of disagreement that were less than 10% between the authors, the mean percentage was taken as the definitive measure of aneurysm coverage. If discordance was greater than 10%, the authors discussed their calculations and repeated the measurement until reaching a consensus. Next, the aneurysm neck coverage percentage was divided by the duration of the experiment, and the fibrin deposition rates (%/min) were calculated for all replicates.

Furthermore, all samples were categorized into 3 groups based on the initial location of fibrin deposition: proximal aneurysm neck, distal aneurysm neck, and non-neck portion of the flow diverter. Fibrin coverage quantification is summarized in Supplementary Fig. 1.

Computational Flow Models

Computational fluid dynamics (CFD) models were constructed for the 4 geometries of the in vitro glass models by using the corresponding STL files. For each geometry, an initial unstructured mesh of tetrahedral elements with an element size resolution of 0.2 mm was generated by using an advancing front approach.[8] Next, flow diverting devices consisting of 48 wires that were 30 μm thick and a braid angle of 90° were virtually deployed in each geometry, with the assumption of no oversizing (i.e., the device reference diameter was 4 mm).[9] Once deployed, the computational mesh was adaptively refined around the device wires and used for flow calculations by using an immersed boundary method on unstructured grids.[10] The refined meshes contained 19, 15, 36, and 68 million elements for the sidewall, curved, paraophthalmic, and bifurcation models, respectively. To simplify the analysis, the flow simulations were carried out under steady conditions by numerically solving the Navier-Stokes equations for an incompressible Newtonian fluid by using an in-house–developed code based on finite elements.[11] Inflow rates of 3, 4, and 5 ml/sec were prescribed at the model inlet by using a parabolic velocity profile. At the model outlet(s), a zero-pressure boundary condition was prescribed. The resulting flows were visualized using 100 streamlines randomly placed within the aneurysm (and propagated in both velocity directions) and velocity vectors on a cut-plane through the center of the aneurysm and the parent artery. Additionally, shear stress was interpolated and visualized on a half cylindrical surface along the flow diverter at the aneurysm neck.

Statistical Analysis

Descriptive and comparative statistics were calculated with statistical software package SPSS version 25.0 for Windows (IBM Corp.). Differences in coverage rates, times, and percentages were examined with ANOVA and post hoc Tukey tests. A p value ≤ 0.05 was considered statistically significant.

Results

A total of 84 replicates (n = 21 in each model) were performed. Of these, 12 were control experiments that were performed under no-flow conditions.

Relationship Between Fibrin Deposition and Flow Rates

The relationship between fibrin deposition and flow rates was examined by using standardized concentrations of fibrin and thrombin: 330 mg/dl and 0.1 U/ml, respectively. No fibrin deposition was observed under no-flow control experiments. The fibrin coverage rate on the aneurysm neck was significantly greater with the 5 ml/sec flow rate as compared with 3 ml/sec for all 4 models (Table 1).

TABLE 1. Aneurysm neck coverage rate changes depending on flow velocities in replicates containing fibrinogen (330 mg/dl) and thrombin (0.1 U/ml)

Model	Aneurysm Neck Coverage Rate, %/min	p Value
Paraophthalmic		
0 ml/sec	0	
3 ml/sec	4.1 ± 3.5	0.3*, **0.006†**
4 ml/sec	5 ± 0.5	**0.037‡**
5 ml/sec	6.7 ± 0.9	
Slightly curved		
0 ml/sec	0	
3 ml/sec	0.13	**0.006***, **0.001†**
4 ml/sec	0.16	**0.004‡**
5 ml/sec	0.19	
Sidewall		
0 ml/sec	0	
3 ml/sec	0.08 ± 0.01	0.058*, **0.007†**
4 ml/sec	0.11 ± 0.01	0.234‡
5 ml/sec	0.12 ± 0.1	
Bifurcation		
0 ml/sec	0	
3 ml/sec	3.9 ± 0.6	**0.036***, **0.004†**
4 ml/sec	6.7 ± 0.9	0.18‡
5 ml/sec	8.4 ± 1.4	

Values are shown as mean or mean ± SD unless indicated otherwise. Boldface type indicates a significant difference according to the post hoc Tukey test.
* 3 ml/sec vs 4 ml/sec.
† 3 ml/sec vs 5 ml/sec.
‡ 4 ml/sec vs 5 ml/sec.

The 5 ml/sec flow rate provided greater fibrin coverage rate than 4 ml/sec for all models; however, the difference was statistically significant only for the curved model (p = 0.004). With the 4 ml/sec flow rate, the neck coverage rate was significantly greater compared to 3 ml/sec for the curved (p = 0.006) and bifurcation (p = 0.036) models. Detailed statistics regarding changes in fibrin coverage time based on flow velocities are presented in Table 1.

Aneurysm Inflow Velocities and Shear Stress After Flow Diverter Deployment

Maximum aneurysm inflow velocities, maximum shear stress, and normalized shear stress values at the device cells were compared using CFD analyses for all models. The paraophthalmic model had the highest inflow velocity of 48.7 cm/sec. The bifurcation model had the highest maximum shear stress (SS) and maximum normalized shear stress values at 843.3 dyne/cm^2 and 35.1 SS/SS_{inflow}, respectively. Detailed CFD results were presented in Table 2. In all models, fibrin started accumulating on the high-flow or high–shear stress areas (Figs. 2–4).

General Fibrin Accumulation Patterns and the Effects of Additives

In all replicates, fibrin began accumulating specifically

TABLE 2. Summary of CFD results

Model	Max Flow Velocity at Aneurysm Neck, cm/sec	Max SS, dyne/cm^2	Max Normalized SS, SS/SS$_{inflow}$	Location of Max SS Zone on Aneurysm Neck	Initial Fibrinogen Deposition Location on Aneurysm Neck
Paraophthalmic	48.7	694.6	28.9	Proximal	Proximal
Bifurcation	31.5	843.3	35.1	Proximal	Proximal
Curved	15	278	11.6	Distal	Distal
Sidewall	4.8	62.9	2.6	Proximal	Proximal

SS = shear stress; SS/SS$_{inflow}$ = normalized shear stress.

at the neck portion of the aneurysm within the flow diverter. Subsequently, other sections of the diverter (i.e., along the parent artery) also became covered by fibrin. In line with the CFD results, fibrin accumulation was particularly noted on the proximal side of the aneurysm neck in the paraophthalmic, sidewall, and bifurcation aneurysm models. Only with the curved model did fibrin accumulation start from the distal side. These initial accumulation sites coincided with aneurysm inflow, as determined from the CFD analyses (proximal neck of the paraophthalmic, sidewall, and bifurcation models and distal neck of the curved model) (Table 2) (Supplementary Figs. 2 and 3). No instent thrombosis occurred.

Fibrin aggregated over the aneurysm neck even in the absence of other coagulation factors. However, complete coverage of the aneurysm neck was only observed in the paraophthalmic aneurysm model for fibrinogen-alone replicates with mean ± SD time to complete coverage of 80 ± 7 minutes. In the other fibrinogen-alone experiments, the neck coverage percentages were 10% for the sidewall model, 30% for the curved model, and 30% for the bifurcation model (Supplementary Table 1). With additives, both the paraophthalmic and bifurcation models demonstrated complete aneurysm neck coverage. Time to coverage ranged between 15 and 33 minutes for the paraophthalmic model and between 12 and 26 minutes for the bifurcation model after the addition of additives (Supplementary Table 1).

Adding thrombin to the fibrinogen solution increased the fibrin coverage rates for all models. Notably, with the addition of thrombin, the bifurcation model exhibited significantly greater fibrin coverage rates than the other models (Table 3). Introducing heparin to the fibrinogen/thrombin solution significantly reduced the neck coverage rates for the paraophthalmic model ($p = 0.002$); however, the differences were not statistically significant for the other models. The inclusion of calcium in the solution of fibrinogen, thrombin, and heparin statistically increased the cov-

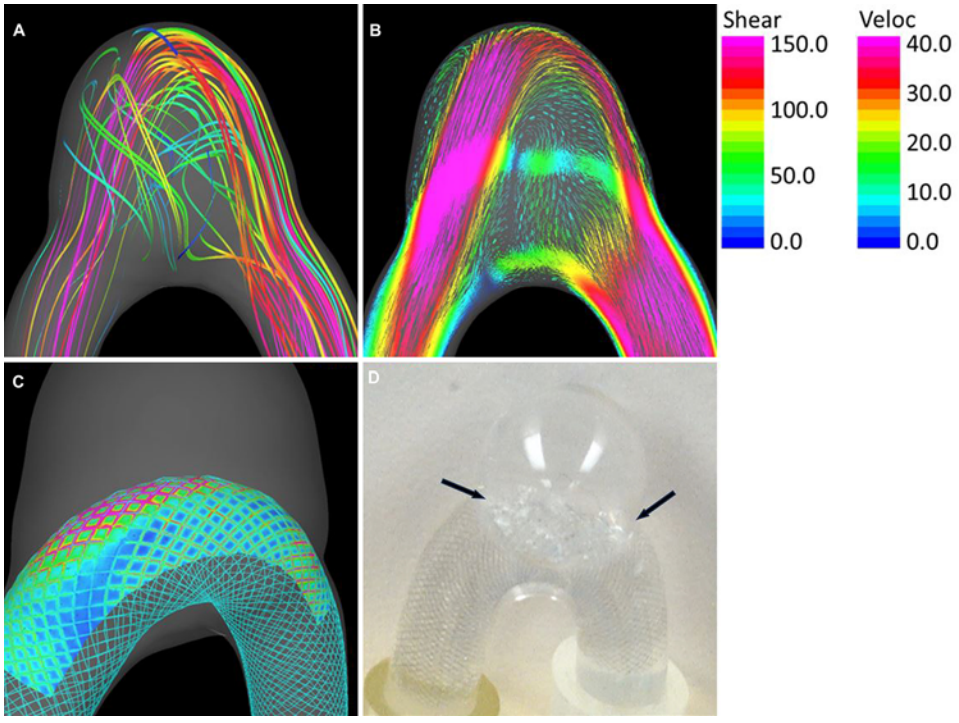

FIG. 2. Intra-aneurysmal flow characteristics after flow diverter deployment of the paraophthalmic aneurysm model (**A and B**). High-flow and high–shear stress zones on the flow diverter (**C**). Fibrin deposition on the aneurysm neck (*arrows*), which corresponds to the high-flow and high–shear stress zones from the CFD analyses (**D**). Veloc = velocity. Figure is available in color online only.

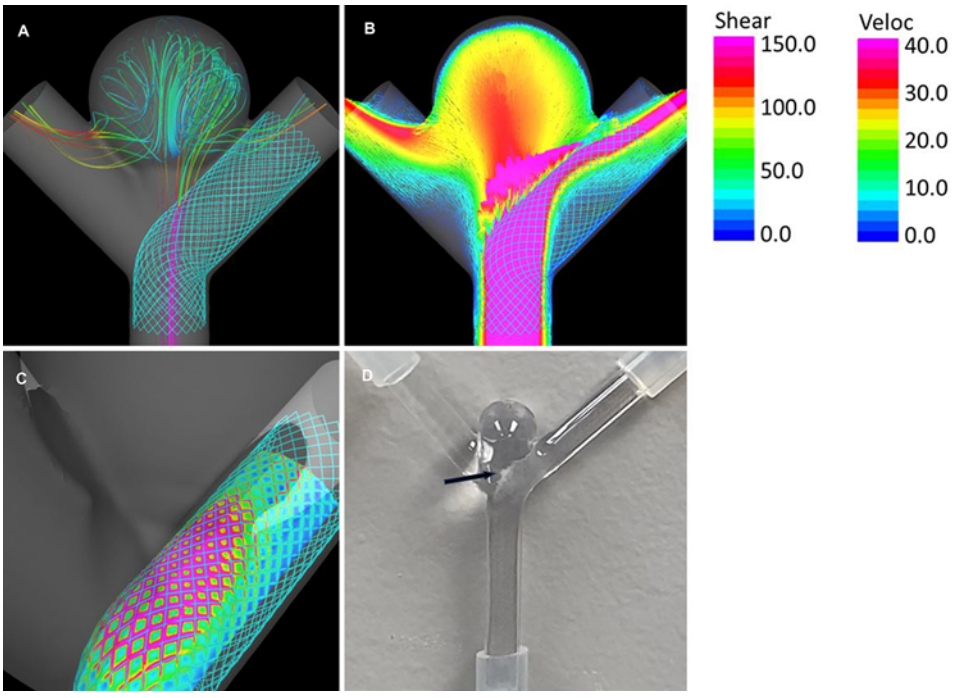

FIG. 3. Intra-aneurysmal flow characteristics after flow diverter deployment of the bifurcation aneurysm model (**A and B**). High-flow and high–shear stress zones on the flow diverter (**C**). Fibrin deposition on the proximal aneurysm neck (*arrow*), which corresponds to the high-flow and high–shear stress zones from the CFD analyses (**D**). Figure is available in color online only.

erage rates for all models, with the exception of the bifurcation model ($p = 0.64$). Detailed results on the impact of additives on fibrin deposition rates are presented in Table 3.

Discussion

Our study revealed several important findings. First, we showed that human fibrinogen converts to fibrin on the surface of flow diverter stents under physiological flow conditions, even without the presence of blood cells, calcium, or thrombin. Second, in our study, models with higher intra-aneurysmal flow or shear stress demonstrated greater and faster fibrin deposition on the neck portion of the flow diverters. Third, CFD analyses revealed that the

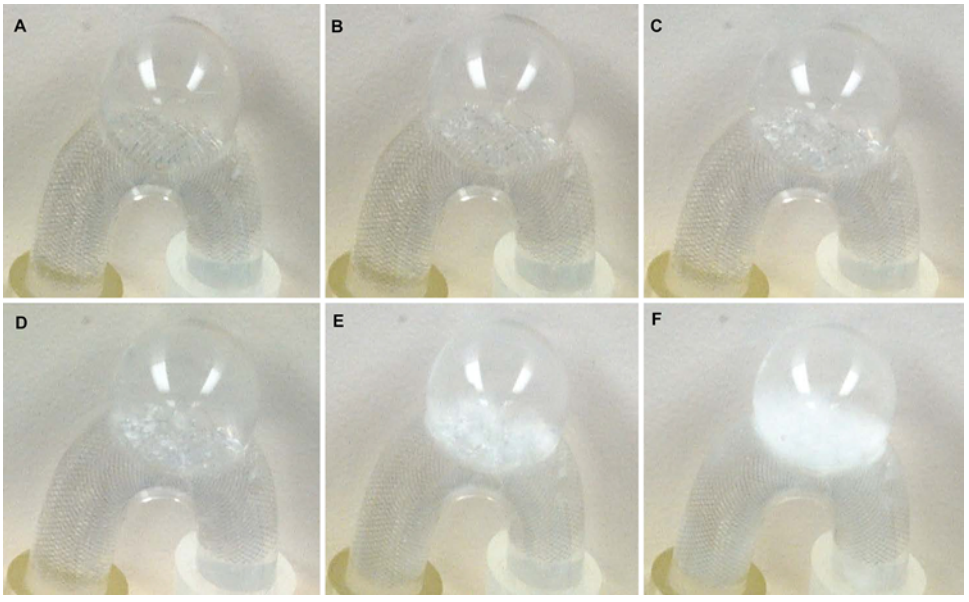

FIG. 4. Gradual fibrin deposition leading to complete aneurysm occlusion. Photographs are shown at baseline (**A**) and after 2 minutes (**B**), 5 minutes (**C**), 7 minutes (**D**), 9 minutes (**E**), and 15 minutes (**F**). Figure is available in color online only.

TABLE 3. Effects of additives on fibrin deposition rates under standardized flow conditions (4 ml/sec)

Model	Aneurysm Neck Coverage Rate, %/min	p Value for Group Comparisons	p Value for Model Comparisons
Paraophthalmic (model A)			
Fibrinogen alone (group 1)	1.25 ± 0.1	**0.001***, **0.003†**, **0.001‡**	**0.001††**, **0.001‡‡**, **0.001§§**
Fibrinogen + thrombin (group 2)	5 ± 0.5	**0.002§**, 0.89¶	**0.001††**, **0.001‡‡**, **0.016§§**
Fibrinogen + thrombin + heparin (group 3)	3.07 ± 0.47	**0.005****	**0.002††**, **0.003‡‡**, **0.002§§**
Fibrinogen + thrombin + heparin + calcium (group 4)	4.7 ± 0.46		0.001††, **0.001‡‡**, **0.001§§**
Sidewall (model B)			
Fibrinogen alone (group 1)	0.03	**0.001***, **0.001†**, **0.001‡**	0.738¶¶, 0.738[a]
Fibrinogen + thrombin (group 2)	0.11	0.134§, **0.001¶**	0.99¶¶, **0.001**[a]
Fibrinogen + thrombin + heparin (group 3)	0.09	**0.001****	0.99¶¶, **0.001**[a]
Fibrinogen + thrombin + heparin + calcium (group 4)	0.15		>0.99¶¶, **0.001**[a]
Curved (model C)			
Fibrinogen alone (group 1)	0.08 ± 0.01	**0.001***, **0.001†**, **0.001‡**	>0.99[b]
Fibrinogen + thrombin (group 2)	0.16	0.053§, **0.001¶**	**0.001**[b]
Fibrinogen + thrombin + heparin (group 3)	0.17	**0.004****	**0.001**[b]
Fibrinogen + thrombin + heparin + calcium (group 4)	0.2		**0.001**[b]
Bifurcation (model D)			
Fibrinogen alone (group 1)	0.08 ± 0.01	**0.001***, **0.001†**, **0.001‡**	
Fibrinogen + thrombin (group 2)	6.7 ± 0.9	0.773§, 0.244¶	
Fibrinogen + thrombin + heparin (group 3)	5.9 ± 1.1	0.64**	
Fibrinogen + thrombin + heparin + calcium (group 4)	8.4 ± 1.4		

Values are shown as mean or mean ± SD unless indicated otherwise. Boldface type indicates statistical significance according to the post hoc Tukey test ($p < 0.05$).
* Group 1 vs group 2.
† Group 1 vs group 3.
‡ Group 1 vs group 4.
§ Group 2 vs group 3.
¶ Group 2 vs group 4.
** Group 3 vs 4.
†† Model A vs B.
‡‡ Model A vs C.
§§ Model A vs D.
¶¶ Model B vs C.
[a] Model B vs D.
[b] Model C vs D.

observed initial fibrin accumulation coincided with the aneurysm inflow zone where the velocity and shear stress tend to be high at the device cells. This indicates that the CFD models, which take into account biological interactions, may provide additional valuable information to assess the likelihood of neck coverage and aneurysm occlusion. These findings are important because they suggest that fibrin could cover a significant proportion of the flow diverter's pores in a short period of time, depending on the flow characteristics of the aneurysm.

Despite the vast flow diversion literature, little is known about how the aneurysm occlusion process begins or proceeds. Several postmortem studies have shown that coils can be covered by fibrin within the early postoperative period.[12–15] Similarly, in our study, the macroscopic fibrin deposition on flow diverter stents began within minutes after deployment. Stamboroski et al. demonstrated that bivalent and monovalent metallic ions may promote fibrinogen precipitation.[16] Additionally, another study by Belisario et al. indicated that this interaction between metal ions and fibrinogen alters the fibrinogen structure and promotes fibrin-myofibroblast or fibrin-platelet adhesion.[17] However, the primary factors driving fibrin accumulation on flow diverter stents had not been previously explored. In our study, fibrin deposited on the flow diverters' necks under physiological flow conditions, even without the addition of blood cells or procoagulants. More importantly, fibrin specifically started accumulating on the high-flow and high–shear stress areas on the flow diverter, resulting in gradual coverage of the aneurysm neck. This has an important potential implication on aneurysm occlusion after flow diverter treatment. It is well known that fibrin provides binding sites for myofibroblasts, which are responsible for collagen production and can promote neointimal layer formation on flow diverter stents. In our study, we deployed flow diverters of the same size across all replicates and utilized glass models with the matched parent artery and aneurysm dimensions. Despite this standardization, we observed significant variations in fibrin deposition on the flow diverters that correlated with dif-

ferences in parent artery curvature and intra-aneurysmal flow rates. Currently, predictors of successful aneurysm occlusion after flow diversion remain largely unexplored. Considering fibrin's crucial role in neoendothelialization and thrombus formation, these disparities in fibrin deposition may contribute to the divergent patient outcomes observed in clinical settings. Further investigation is needed to elucidate fibrin's specific role in aneurysm occlusion after flow diversion.

The most commonly used in vitro flow diverter model consists of a silicone aneurysm model and a flow loop, and it uses a glycerol-based fluid to mimic the lubricity of blood.[18–20] In this previous model, a contrast bolus is administered after device deployment, and contrast intensity is measured for approximately 20 seconds. High contrast intensity indicates greater stagnation and more efficacy. Although this model provides a useful platform for preclinical testing, its real-world efficacy remains unexplored, as flow diverter–induced aneurysm occlusion may take months or sometimes years. Our model has two main advantages over the available in vitro flow diversion models. First, instead of focusing on a short period of time, our model allows real-time visualization of gradual aneurysm occlusion. Second, fibrinogen provides binding sites for myofibroblasts, which produce collagen and are the main drivers of neointimal layer formation. Therefore, implementing human fibrinogen in benchtop models may provide more realistic preclinical testing platforms that consider biological factors.[21]

Gester et al. investigated the mechanism and characteristics of flow diverter–induced aneurysm thrombosis using anticoagulated pig blood.[22] Incorporating whole blood into an in vitro model can provide valuable insights into the role of blood cells and other components in aneurysm occlusion after flow diverter treatment. However, it is important to note that hemolysis is inevitable under in vitro conditions. Additionally, thrombosis starts immediately under ex vivo conditions, and therefore these models require high doses of anticoagulants. In our study, we performed a total of 84 experiments with 3 replicates for each treatment arm, and we obtained consistent results, as supported by the low standard deviations. Also, our fibrinogen-based model successfully reflected changes in parent artery or intra-aneurysmal flow rates and the influence of biological components such as thrombin, calcium, and heparin. Therefore, our findings suggest that the human fibrinogen–based flow diverter model may provide more reproducible and consistent results than animal blood–based models.

Our study has several limitations. First, our model does not consider cellular interactions and may not represent known or currently unknown coagulant or anticoagulant mechanisms. Therefore, it is important to note that aneurysm neck coverage times are only shared as a reference for our in vitro model. Second, fibrin serves as a substrate for cell binding, potentially influencing device neoendothelialization. However, neoendothelialization is a complex process that may commence as late as 7 days after flow diversion.[3,23] Third, glass models are rigid, in contrast to blood vessels, and this may have affected the flow characteristics. Fourth, our test flow diverter had cobalt-chromium wires. Fibrin deposition characteristics may vary for different metal ions. Lastly, we used a pulsatile pump for our experiments, which may limit representation of in vivo flow characteristics.

Conclusions

Predictors of flow diversion success remain largely unexplored. Our human fibrinogen–based model may address the important limitations of the available benchtop flow diverter–testing platforms. Additionally, our results suggest that, depending on aneurysm anatomy, fibrinogen alone can completely cover the aneurysm neck and lead to aneurysm occlusion. Further research is needed to understand the role of fibrinogen in aneurysm occlusion after flow diverter treatment.

Acknowledgments

This study was funded by the National Institute of Neurological Disorders and Stroke (NS076491).

References

1. Kattula S, Byrnes JR, Wolberg AS. Fibrinogen and fibrin in hemostasis and thrombosis. *Arterioscler Thromb Vasc Biol*. 2017;37(3):e13-e21.
2. Weisel JW, Litvinov RI. Fibrin formation, structure and properties. *Subcell Biochem*. 2017;82:405-456.
3. Kadirvel R, Ding YH, Dai D, Rezek I, Lewis DA, Kallmes DF. Cellular mechanisms of aneurysm occlusion after treatment with a flow diverter. *Radiology*. 2014;270(2):394-399.
4. Ravindran K, Casabella AM, Cebral J, Brinjikji W, Kallmes DF, Kadirvel R. Mechanism of action and biology of flow diverters in the treatment of intracranial aneurysms. *Neurosurgery*. 2020;86(Suppl 1):S13-S19.
5. Becske T, Kallmes DF, Saatci I, et al. Pipeline for uncoilable or failed aneurysms: results from a multicenter clinical trial. *Radiology*. 2013;267(3):858-868.
6. Meyers PM, Coon AL, Kan PT, Wakhloo AK, Hanel RA. SCENT trial. *Stroke*. 2019;50(6):1473-1479.
7. Shehata MA, Ibrahim MK, Ghozy S, et al. Long-term outcomes of flow diversion for unruptured intracranial aneurysms: a systematic review and meta-analysis. *J Neurointerv Surg*. 2023;15(9):898-902.
8. Cebral JR, Castro MA, Appanaboyina S, Putman CM, Millan D, Frangi AF. Efficient pipeline for image-based patient-specific analysis of cerebral aneurysm hemodynamics: technique and sensitivity. *IEEE Trans Med Imaging*. 2005;24(4):457-467.
9. Mut F, Cebral JR. Effects of flow-diverting device oversizing on hemodynamics alteration in cerebral aneurysms. *AJNR Am J Neuroradiol*. 2012;33(10):2010-2016.
10. Appanaboyina S, Mut F, Löhner R, Putman C, Cebral J. Simulation of intracranial aneurysm stenting: techniques and challenges. *Comput Methods Appl Mech Eng*. 2009;198(45-46):3567-3582.
11. Mut F, Aubry R, Löhner R, Cebral JR. Fast numerical solutions of patient-specific blood flows in 3D arterial systems. *Int J Numer Methods Biomed Eng*. 2010;26(1):73-85.
12. Bavinzski G, Talazoglu V, Killer M, et al. Gross and microscopic histopathological findings in aneurysms of the human brain treated with Guglielmi detachable coils. *J Neurosurg*. 1999;91(2):284-293.
13. Groden C, Hagel C, Delling G, Zeumer H. Histological findings in ruptured aneurysms treated with GDCs: six examples at varying times after treatment. *AJNR Am J Neuroradiol*. 2003;24(4):579-584.
14. Stiver SI, Porter PJ, Willinsky RA, Wallace MC. Acute hu-

man histopathology of an intracranial aneurysm treated using Guglielmi detachable coils: case report and review of the literature. *Neurosurgery*. 1998;43(5):1203-1208.
15. Brinjikji W, Kallmes DF, Kadirvel R. Mechanisms of healing in coiled intracranial aneurysms: a review of the literature. *AJNR Am J Neuroradiol*. 2015;36(7):1216-1222.
16. Stamboroski S, Boateng K, Lierath J, et al. Influence of divalent metal ions on the precipitation of the plasma protein fibrinogen. *Biomacromolecules*. 2021;22(11):4642-4658.
17. Belisario MA, Di Domenico C, Pelagalli A, Della Morte R, Staiano N. Metal-ion catalyzed oxidation affects fibrinogen activity on platelet aggregation and adhesion. *Biochimie*. 1997;79(7):449-455.
18. Dholakia RJ, Kappel AD, Pagano A, et al. In vitro angiographic comparison of the flow-diversion performance of five neurovascular stents. *Interv Neuroradiol*. 2018;24(2):150-161.
19. Oliver AA, Bilgin C, Vercnocke AJ, et al. Benchtop proof of concept and comparison of iron- and magnesium-based bioresorbable flow diverters. *J Neurosurg*. 2022;139(1):150-156.
20. Sadasivan C, Fiorella D. Preliminary in vitro angiographic comparison of the flow diversion behavior of Evolve and Pipeline devices. *J Neurointerv Surg*. 2020;12(6):616-620.
21. Dejana E, Lampugnani MG, Giorgi M, Gaboli M, Marchisio PC. Fibrinogen induces endothelial cell adhesion and spreading via the release of endogenous matrix proteins and the recruitment of more than one integrin receptor. *Blood*. 1990; 75(7):1509-1517.
22. Gester K, Lüchtefeld I, Büsen M, et al. In vitro evaluation of intra-aneurysmal, flow-diverter-induced thrombus formation: a feasibility study. *AJNR Am J Neuroradiol*. 2016;37(3):490-496.
23. Liu W, Dai D, Ding YH, et al. Cellular responses to flow diverters in a tissue-engineered aneurysm model. *J Neurointerv Surg*. 2021;13(8):746-751.
24. Dai D, Bilgin C, Ding Y, et al. How the elastase-induced rabbit aneurysm heals following flow diverter treatment: a histopathological study. *J Neurosurg*. Published online May 17, 2024. doi:10.3171/2024.2.JNS232262

Disclosures

Dr. Cebral reported research grants from NIH during the conduct of the study. Dr. Kallmes reported grants from Medtronic, MicroVention, Balt, and Stryker; and holds equity in Monarch Biosciences outside the submitted work. Dr. Kadirvel reported NIH grant nos. NS076491 and R21 NS128199 during the conduct of the study; and grants from Bionaut Labs, MIVI Biosciences, Piraeus Medical, Cerenovus, Sensome, and Styrker; and material support from Medtronic outside the submitted work.

Author Contributions

Conception and design: Bilgin, Bayraktar, Cebral, Kallmes, Kadirvel. Acquisition of data: Bilgin, Bayraktar, Oliver, Li, Cebral. Analysis and interpretation of data: all authors. Drafting the article: Bilgin, Cebral, Kallmes, Kadirvel. Critically revising the article: Bilgin, Oliver, Li, Cebral, Kallmes, Kadirvel. Reviewed submitted version of manuscript: Bilgin, Bayraktar, Oliver, Li, Cebral, Kallmes, Kadirvel. Approved the final version of the manuscript on behalf of all authors: Bilgin. Statistical analysis: Bilgin, Kallmes. Administrative/technical/material support: Bayraktar, Cebral, Kallmes, Kadirvel. Study supervision: Cebral, Kallmes, Kadirvel.

Supplemental Information

Online-Only Content

Supplemental material is available with the online version of the article.

Supplementary Figures and Table. https://thejns.org/doi/suppl/10.3171/2024.4.JNS232567.

Correspondence

Cem Bilgin: Mayo Clinic, Rochester, MN. bilgin.cem@mayo.edu.